



Effects of reconstruction methods on dose distribution for lung stereotactic body radiotherapy treatment plans

Yagiz Yedekci¹ · Pervin Hurmuz¹ · Gökhan Ozyigit¹

Received: 30 March 2022 / Accepted: 4 December 2022 / Published online: 16 December 2022
© The Author(s), under exclusive licence to Springer-Verlag GmbH Germany, part of Springer Nature 2022

Abstract

The aim of the present study was to investigate the effect of tumour motion on various imaging strategies as well as on treatment plan accuracy for lung stereotactic body radiotherapy treatment (SBRT) cases. The ExacTrac gating phantom and paraffin were used to investigate respiratory motion and represent a lung tumour, respectively. Four-dimensional computed tomography (4DCT) imaging was performed, while the phantom was moving sinusoidally with 4 s cycling time with three different amplitudes of 8, 16, and 24 mm. Reconstructions were done with maximum (MIP) and average intensity projection (AIP) methods. Comparisons of target density and volume were performed using two reconstruction techniques and references values. Volumetric modulated arc therapy (VMAT) and intensity modulated radiation therapy (IMRT) were planned based on reconstructed computed tomography (CT) sets, and it was examined how density variations affect the dose-volume histogram (DVH) parameters. 4D cone beam computed tomography (CBCT) was performed with the Elekta Versa HD linac imaging system before irradiation and compared with 3D CBCT. Thus, various combinations of 4DCT reconstruction methods and treatment alignment methods have been investigated. Point measurements as well as 2 and 3D dose measurements were done by optically stimulated luminescence (OSL), gafchromic films, and electronic portal imaging devices (EPIDs), respectively. The mean volume reduction was 7.8% for the AIP and 2.6% for the MIP method. The obtained Hounsfield Unit (HU) values were lower for AIP and higher for MIP when compared with the reference volume density. In DVH analysis, there were no statistical differences for $D_{95\%}$, $D_{98\%}$, and D_{mean} ($p > 0.05$). However, $D_{2\%}$ was significantly affected by HU changes ($p < 0.01$). A positional variation was obtained up to 2 mm in moving direction when 4D CBCT was applied after 3D CBCT. Dosimetric measurements showed that the main part of the observed dose deviation was due to movement. In lung SBRT treatment plans, $D_{2\%}$ doses differ significantly according to the reconstruction method. Additionally, it has been observed that setups based on 3D imaging can cause a positional error of up to 2 mm compared to setups based on 4D imaging. It is concluded that MIP has advantages over AIP in defining internal target volume (ITV) in lung SBRT applications. In addition, 4D CBCT and 3D EPID dosimetry are recommended for lung SBRT treatments.

Keywords Lung SBRT · 4DCT · 4DCBCT · 3D in vivo dosimetry

Introduction

Stereotactic body radiation therapy (SBRT) involves precisely delivering high radiation doses to cancer cells while minimizing irradiation of the surrounding normal tissues. The efficacy of SBRT in the treatment of early stage lung cancer has led to the widespread use of this treatment modality in such cases (Taremi et al. 2012; Simone et al. 2013;

Timmerman et al. 2013; Chang et al. 2015). However, respiratory-induced motions are one of the main challenges in lung SBRT applications (Admiraal et al. 2008). Motion management is an essential part of lung SBRT applications and it is critical for better therapeutic outcomes (Brandner et al. 2017). Modern radiation therapy technologies carefully address this issue from the definition of the target volume to the delivery of treatment. Currently, the respiratory motion of the lung can be determined by four-dimensional computed tomography (4DCT) scans (Slotman 2006). 4DCT imaging involves scanning patients at different respiratory phases. This procedure causes higher imaging doses than 3D CT, but it generally reduces the target volumes (Vedam 2002;

✉ Yagiz Yedekci
yagiz.yedekci@hacettepe.edu.tr

¹ Department of Radiation Oncology, Faculty of Medicine, Hacettepe University, 06100, Sıhhiye, Ankara, Turkey

Nakamura et al. 2008). In 4DCT, the target is delineated in each scanned data set, so that the whole tumour trajectory can be described. Since this method is time-consuming, some clinicians prefer post-processing tools to generate internal target volume (ITV) from 4DCT datasets. Treatment planning systems may provide different post-processing methods for this process. It is well known that the quality of the reconstructed 4DCT images depends on the projection methods (Bradley et al. 2006; Zamora et al. 2010). The most common post-processing methods, maximum intensity projection (MIP), and average intensity projection (AIP) reflect the maximum and mean data values within each voxel of volumetric data of the bins of the 4D scan (Underberg et al. 2005).

Irradiation of the target with high precision is as important as determining the target with high accuracy. Cone-beam computed tomography (CBCT) provides 3D imaging and requires high precision patient setup before treatment (Purdie et al. 2007). For moving targets, 4D CBCT imaging is an alternative including an advanced image guided radiation therapy (IGRT) modality for visualization of target and accurate irradiation (Thengumpallil et al. 2016; Zhi et al. 2020). IGRT allows to visualize whether the tumour moves in the region of ITV or not (Sweeney et al. 2012). However, it costs much more time when compared with standard CBCT practices.

Respiration might cause uncertainties for dynamic treatment techniques in dose delivery, due to a simultaneous movement of machine parts and target (Sarudis et al. 2022). Verification of the delivered doses could be performed with point dose, 2D dose, and 3D dose measurements. 3D dosimetry has many advantages over point dosimetry and 2D dosimetry, and 3D doses can be measured in vivo by Electronic Portal Imaging Devices (EPIDs) (Low 2015).

The purpose of the present study was to investigate the impact of reconstruction techniques on target volume delineation, DVH parameters, and dose distribution.

Materials and methods

Phantom design

The ExacTrac[®] gating phantom (BrainLAB[™], Munich, Germany) and a rectangular prism-shaped paraffin volume with dimensions 2 cm × 2 cm × 1 cm (4 cm³) were used to simulate the patient's sinusoidal respiratory motion and a lung tumour, respectively. The paraffin was bisected and a cavity was created for optically stimulated luminescence (OSL) NanoDots[™] (Landauer, Inc., Glenwood, IL, USA) dosimeters to measure the absorbed dose (Fig. 1). The paraffin was centrally positioned in the phantom during imaging and irradiation (Fig. 1).



Fig. 1 Optically Stimulated Luminescence (OSL) dosimeter inside the paraffin material used to simulate a tumour, and the phantom setup used for imaging and irradiations

Imaging and delineation of internal target volume

Computed tomography (CT) images of the phantom were acquired using helical scanning with an Aquilion LB (Toshiba Medical Systems, Otawara, Japan) multislice CT scanner including 28 curved detector modules. All 4DCT images for the phantom measurements were acquired and reconstructed with the following parameters: slice collimation – 16 × 1.0 mm, helical pitch – 1.2, rotation time – 0.5 s, matrix – 512 × 512, tube voltage – 120 kV, and tube current – 100 mA.

During the experiments, the respiratory phantom moved sinusoidally with a cycling time of 4 s and three different amplitudes of 8, 16, and 24 mm (representing low, medium, and high amplitude). The scans were repeated for 3, 6, and 10 phases. 4DCT image sets were reconstructed by the MIP and AIP methods. Reconstruction was performed with the RayStation Version 8A treatment planning system (TPS) (RaySearch Laboratories, Stockholm, Sweden). Table 1 shows details on phase angles of image acquisition. In the table, “free moving” represents the sinusoidal movement of the phantom. This means that the images were obtained, while the phantom was moving. The phase angles are the angles in the sinusoidal movement which represent different positions of the phantom.

Initially, the simulated tumour was delineated as ITV on each 4DCT slice in the lung window (between – 600 and 1600 HU) by visual inspection. The delineation was performed by an experienced radiation oncologist. Then, ITV and mean Hounsfield unit (HU) values were recorded and compared with reference values to investigate the imaging

Table 1 Image acquisition phases

Movement phases	
3 phases	90° 270° Free moving
6 phases	90° 180° 270° 0° 90° Free moving
10 phases	90° 135° 180° 225° 270° 315° 0° 45° 90° Free moving

accuracy of the applied methods. The reference value for ITV was calculated based on movement amplitude. In the presence of motion, the reference ITV values were calculated by Eq. 1

$$ITV = A \times (B + L) \times C, \quad (1)$$

where A , B , and C represent the edge size of the rectangular prism-shaped paraffin volume in the lateral, longitudinal, and vertical direction, respectively; L represents the maximum displacement of the phantom in direction of the B axis.

Mean reference HU values of the ITV were obtained from scanned data of the static phantom.

Treatment planning

In this study, all treatment plans were obtained with the RayStation version 8A TPS. The Raystation dose calculation engine includes inhomogeneity corrections. The clinical dose engine for photons is called “Collapsed Cone” (CC). During optimization, a simplified dose engine called “Singular Value Decomposition” (SVD) was used. The VMAT plans with two arcs (from 270 to 90° gantry angles, in clockwise and counter-clockwise direction) were created on reconstructed CTs. Also, IMRT with five fields (Gantry angles: 0, 60, 100, 260, and 300°) were planned. The prescription dose was 10 Gy. $D_{95\%}$, $D_{98\%}$, D_{mean} , and $D_{2\%}$ doses of the ITV were recorded for dose-volume histogram (DVH) analysis. $D_{95\%}$, $D_{98\%}$, and $D_{2\%}$ are doses received by 95, 98, and 2% of the ITV volume, respectively. Furthermore, the obtained treatment plans were recalculated by changing the HU of the ITV with to the reference HU value. This was done to investigate how any HU differences due to the reconstruction method might affect the investigated dose-volume parameters ($D_{95\%}$, $D_{98\%}$, D_{mean} , and $D_{2\%}$).

CBCT imaging

CBCT imaging was performed using the Elekta Versa HD linac imaging system (XVI System, Elekta AB, Stockholm, Sweden) mounted on a gantry perpendicular to the treatment beam. The lung protocol was selected for 3D CBCT. The selected lung protocol performed a 360° rotation in 2 min with a 40 mA tube current. The symmetry protocol was selected for 4D CBCT. This protocol performed a 200° gantry rotation in 4 min with 20 mA tube current and 120 kV

tube voltage. 3D and 4D CBCT images were compared for moving targets and the isocenter shifts were recorded.

Irradiation and dosimetric analysis

The Elekta Versa HD (Elekta AB, Stockholm, Sweden) treatment machine was used for the delivery of treatment plans. Point dose measurements were performed with OSL dosimeters. 2D dose distributions were measured with EBT3 gafchromic films. 3D EPID dosimetry was also performed using the commercially available algorithm iViewDoseTM v.1.0.1 (Elekta, Stockholm, Sweden).

The moving phantom was irradiated after 4D CBCT imaging. Then, it was paused at the isocenter, the irradiated OSL dosimeter (OSLD) was removed and a new OSLD was inserted. After that, the imaging was repeated and the phantom was irradiated again in a stationary position. All measurements were made three times and the mean value of the measurements was calculated. The same workflow was repeated for the EBT3 film measurements and EPID dosimetry. Point dose measurements were compared with TPS doses. Gamma evaluation was used for analyzing the film and 3D EPID results with 3% global dose difference/3 mm distance to agreement, 50% threshold, and 90% acceptance criteria.

The gamma passing rate was calculated using Eq. 2

$$\gamma(r_m, r_c) = \sqrt{\frac{(r_m - r_p)^2}{\delta r_m^2} + \frac{(d_m - d_p)^2}{\delta d_m^2}}, \quad (2)$$

where δr_m distance to agreement (DTA) criterion, δd_m dose difference criterion, m measured dose, and p planned dose (Childress and Rosen 2003).

It was also investigated whether the tumour volume was covered with a 95% isodose line.

Results

4DCT imaging

Table 2 displays mean HU values and ITVs for various 4DCT image sets and different phantom movements. Data in Table 2 suggest that ITVs were lower than the reference volumes calculated according to Eq. 1. In particular, the

Table 2 Internal Target Volumes (ITVs) and density of ITVs with references values for different reconstruction methods and tumour amplitudes

		ITV volume(cc)					
		Low amplitude		Medium amplitude		High amplitude	
		Reference	4DCT	Reference	4DCT	Reference	4DCT
3 phases	MIP	5.6	5.5	7.2	7.2	8.8	8.7
	AIP		5		6.7		8.2
6 phases	MIP		5.4		7.1		8.4
	AIP		5.2		6.6		8
10 phases	MIP		5.6		7.1		8.8
	AIP		5.4		6.6		8

		Density (HU)					
		Low amplitude		Medium amplitude		High amplitude	
		Reference	4DCT	Reference	4DCT	Reference	4DCT
3 phases	MIP	– 281	– 198	– 281	– 245	– 281	– 227
	AIP		– 472		– 602		– 621
6 phases	MIP		– 182		– 172		– 252
	AIP		– 379		– 547		– 634
10 phases	MIP		– 184		– 191		– 227
	AIP		– 413		– 558		– 621

cc cm³, AIP average intensity projection, MIP mean intensity projection

mean volume reduction was 7.8% for the AIP and 2.6% for the MIP methods. No significant volumetric difference was observed depending on the phase group. Furthermore, the results show that the density of ITVs varied with the projection method and motion amplitude. The HU values were lower for the AIP method compared to the reference value. On the other hand, HU values for the MIP technique were found to be higher than the reference volume density. As the amplitude of motion increased, HU values decreased.

Treatment planning and DVH analysis

Table 3 shows $D_{95\%}$, $D_{98\%}$, D_{mean} and $D_{2\%}$ values for ITVs. DVH analysis for ITV doses showed that there were no significant differences for $D_{95\%}$, $D_{98\%}$, and D_{mean} ($p > 0.05$). However, $D_{2\%}$ was significantly affected by HU changes ($p < 0.01$). Figure 2 visualizes the differences in the high-dose region. The figure shows how the dose distribution depends on HU values in IMRT planning for 10-phase imaging. While mean 0.5% dose differences were calculated for $D_{95\%}$ doses of the IMRT plans, this deviation was 3.7% for VMAT plans. A similar result was also observed for $D_{98\%}$ values: the dose differences for $D_{98\%}$ values of IMRT and VMAT plans were 0.5 and 4.7%, respectively ($p < 0.01$). The mean deviation was almost the same for D_{mean} and $D_{2\%}$.

CBCT imaging

Initially, 3D CBCT was performed, while the phantom was moving for setup validation. It was ensured that the movement of the paraffin was within the ITV. Then, 4D CBCT was performed and phantom shifts were recorded according to the 3D CBCT setup. There were no rotational corrections. However, up to 2 mm shifts were observed in the moving direction (Fig. 3). After position correction with 4D CBCT, the tumour was observed to be within the ITV region for all 4DCT acquisition modalities.

Irradiation and dosimetric analysis

Table 4 shows the result of point dose measurements with OSLD in percentage. TPS data were taken as the reference value. The results show that stationary phantom measurements are compatible with TPS data within $\pm 2\%$. On the other hand, for the moving phantom measurements deviated from TPS data by up to 12%.

Table 5 displays gamma analysis results for film and 3D EPID measurements. Gamma passing rates increased when the phantom was irradiated in a stationary position in both 2 and 3D measurements. Also, it was observed that the gamma passing rate in 3D in vivo EPID dosimetry decreased.

Table 3 Effects of Hounsfield (HU) differences on dose-volume histogram (DVH) parameters

	Reproduction method	Treatment modality	ITV doses(Gy)							
			D ₉₅		D ₉₈		D _{mean}		D ₂	
			Initial plan	Modified plan	Initial plan	Modified plan	Initial plan	Modified plan	Initial plan	Modified plan
3 phases	MIP	IMRT	10.0	9.8	9.9	9.8	10.0	10.0	10.1	10.2
		VMAT	10.0	9.6	9.9	9.4	10.0	10.0	10.0	10.2
	AIP	IMRT	10.0	10.0	9.9	9.9	10.0	10.2	10.1	10.6
		VMAT	9.7	9.8	9.6	9.7	10.0	10.1	10.3	10.4
6 phases	MIP	IMRT	9.9	9.9	9.9	9.9	10.0	10.0	10.1	10.2
		VMAT	10.0	9.6	10.0	9.5	10.0	10.0	10.1	10.3
	AIP	IMRT	10.0	10.0	9.9	9.9	10.0	10.1	10.1	10.5
		VMAT	9.9	9.4	9.8	9.2	10.0	10.0	10.1	10.4
10 phases	MIP	IMRT	10.0	9.9	9.9	9.9	10.0	10.0	10.1	10.1
		VMAT	9.5	9.9	9.3	9.9	10.0	10.0	10.4	10.1
	AIP	IMRT	9.9	10.0	9.9	9.9	10.0	10.2	10.1	10.7
		VMAT	10.0	9.5	9.9	9.4	10.0	10.1	10.1	10.4

AIP average intensity projection, MIP mean intensity projection, ITV internal target volume

Discussion

In the current study, the effects of various post-processing methods to create 4DCT images in lung SBRT were evaluated. It was observed that ITVs obtained from post-processed images were lower than the corresponding reference values. The volume reduction was much higher when the AIP method was used than when the MIP method was used. This is consistent with the results of previous studies in which it was reported that MIP-based ITV was widely adapted due to its excellent correlation with ITV (Underberg et al. 2006; Wang et al. 2018). However, when a tumour is adjacent to high-density tissues, MIP-based ITV delineation may fail to visualize the full extent of the ITV (Muirhead et al. 2008). In such situations, AIP-based ITV delineation may be chosen. Furthermore, the density of ITV varied with projection method. The results showed that ITV densities obtained with the AIP method were two times lower than those obtained with the MIP method. The volume reduction observed when the AIP technique was used may be associated with low HU values of ITV in AIP, since the decrease in density of ITV affects the visibility of the target.

Lung SBRT is a challenging technique in terms of imaging to dose delivery. It should be carefully applied to ensure consistency between planned and delivered dose. Previously, geometrical and dosimetrical uncertainties in hypo-fractionated radiotherapy of the lung were discussed in detail by Schwarz et al. (2017). Technical aspects were presented and discussed, and recent developments were summarized. Dose calculation algorithms, such as convolution algorithms, Monte Carlo approaches, and solutions of the transport equation, were considered appropriate to handle small and heterogeneous geometries that make dose calculations difficult. In the current study, the collapsed cone convolution algorithm (Type B) was used, which is one of the recommended dose calculation algorithms. It should be noted, however, that using this algorithm, there is still about a 3% dose uncertainty when compared with Monte Carlo simulations (Chopra et al. 2019). Using Type C algorithms might therefore provide more realistic results.

Previously, Bradley and co-workers also found that MIP-defined targets were larger than AIP-defined targets (Bradley et al. 2006). In addition to their study, the present work has shown that tumour size defined in MIP is closest to the actual physical size of the target, as it is a well-known volume used in the experiments of the present study. It was also found that as the amplitude of the movement increased, the density of ITV decreased. Image blurring due to the amplitude can cause differences in density. Previously, Underberg and co-workers reported that

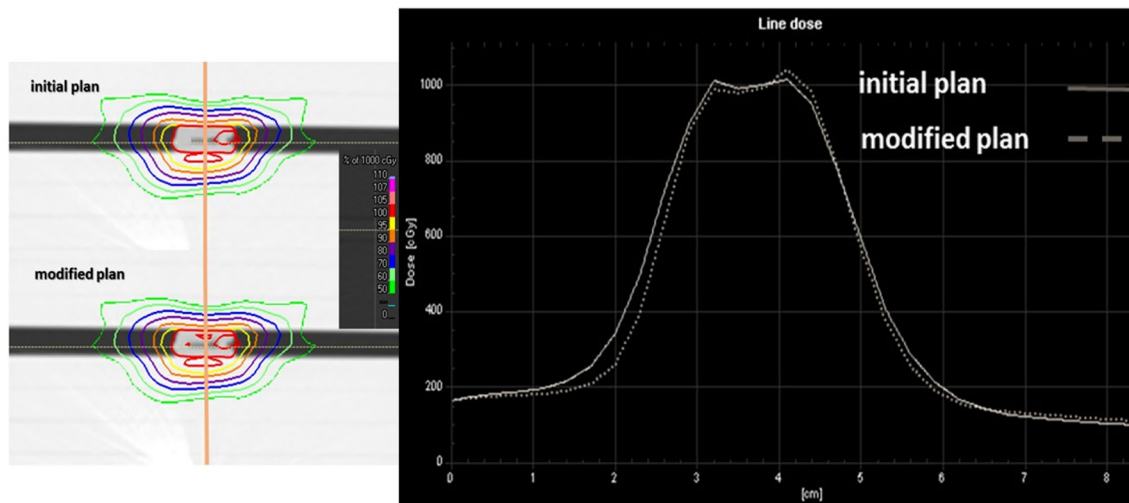


Fig. 2 Dose distribution for the initial and modified Intensity Modulated Radiation Therapy (IMRT) plans of the 10-phase imaging

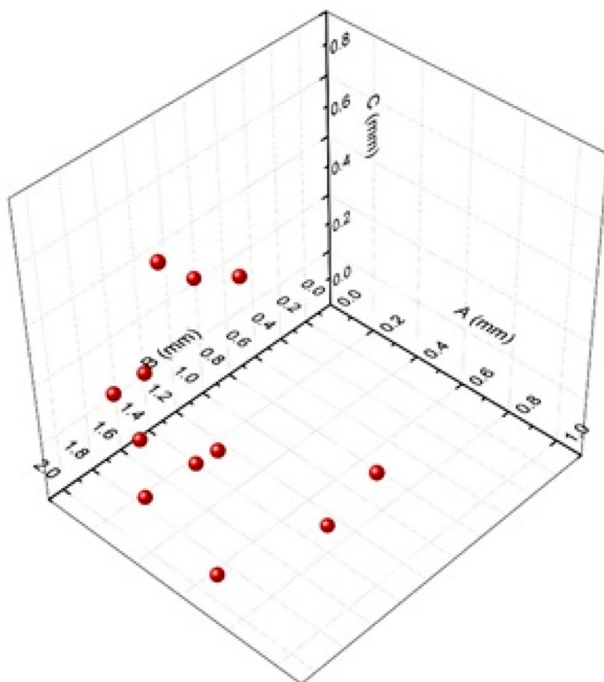


Fig. 3 Recorded absolute values of phantom shifts for 4D CBCT following 3D CBCT. **A**, **B**, and **C** represent deviation in lateral direction, phantom movement direction, and vertical direction, respectively

there were no significant ITV differences in eight patients between ten phases 4DCT and six phases multiscan CT (Underberg et al. 2004). However, they mentioned considerably larger ITVs for 10-phase 4DCT in two patients whose tumour exhibited the greatest mobility. There was no ITV and density difference for 4DCT images created with different phase numbers in the present study. The

Table 4 Results of point dose measurements with optically stimulated luminescence (OSL) dosimeters in percentage

	Low amplitude	Medium amplitude	High amplitude
VMAT	109.5	106.3	98.0
VMAT stationary	100.5	100.0	102.0
IMRT	105.4	99.0	102.6
IMRT stationary	99.5	101.0	98.5

Table 5 Gamma analysis results

		Total gamma results			
		Film		3D EPID	
		MIP	AIP	MIP	AIP
Moving phantom	VMAT	90.7	92.2	80.4	81.4
	IMRT	91.5	91.8	82.5	81.8
Stationary phantom	VMAT	95.2	96.6	90.6	94.0
	IMRT	94.2	93.2	96.8	92.1

AIP average intensity projection, *MIP* mean intensity projection

reason may be the simple motion of the phantom in the present experiment. In the moving phantom, the replacement of the target was only in one direction with a maximum displacement of 24 mm. In contrast, however, a patient's tumour motion can be even larger and in three dimensions. This simplification in tumour motion represents a limitation of the present study.

As another limitation of the present study, the comparison of the EPID reconstructed with the TPS dose distribution was done by 3D gamma analysis with a 3% global dose

difference/3 mm DTA. This gamma criterion was chosen according to data previously published by Yedekci and co-workers (Yedekci et al. 2019). These authors performed 3D gamma analysis for in vivo EPID dosimetry for prostate SBRT. However, in a recent study, it was recommended to perform 2D gamma analysis with 2% global dose difference/2 mm DTA for SBRT (Miften et al. 2018).

In the treatment planning stage, the present study investigated how the above-mentioned density changes affect the target's DVH parameters. Differences in the ITV HU value result in inaccuracies in ITV electron densities. This may significantly affect the dose calculations (Giantsoudi et al. 2017). Mohatt and co-workers suggested that the Analytical Anisotropic Algorithm (AAA) predicted a greater than 2% dose error at the isocenter over a target density variation of 200 HU. In the present experiment, HU differences reached up to 400 HU and the Collapse Cone Algorithm predicted significant differences of up to 5% for $D_{2\%}$ values. In other studies, on average, about 3% dose differences were observed for $D_{95\%}$ and $D_{98\%}$ values, and smaller differences were seen for D_{mean} values (Tian et al. 2012; Liu et al. 2016; Mohatt et al. 2018). The findings of the present study are comparable with those obtained in these studies. However, a statistically significant difference was only observed for $D_{2\%}$ doses.

When 4D CBCT was performed following 3D CBCT, treatment couch alignment was needed for the moving phantom. This demonstrates the importance of imaging modality for moving targets. Consequently, treatment planners should consider the imaging method of the setup. Additional PTV margins are needed if imaging is done with 3D CBCT. Previous studies have also shown that 4D CBCT ensures a reasonable dose and better image quality when moving targets are involved compared to 3D CBCT (Jiang et al. 2012; Sweeney et al. 2012; Thengumpallil et al. 2016).

Results of point dose measurements at the isocenter were in agreement with TPS doses within $\pm 2\%$ dose deviation, which is acceptable for a stationary phantom. The dose variation increased up to 9.5% for a moving phantom. The results of gafchromic film measurements showed good agreement with TPS doses, for a moving phantom, with a mean passing rate of 91.6%. In contrast, the mean passing rate for a static phantom was 94.8%. However, hotspots of up to 110% within the ITV were observed in gamma analysis for a moving phantom. Previously, many investigators studied this subject for mobile targets (Kubo et al. 2018; Pan et al. 2019). They attributed the observed dose differences to the interplay effect. The influence of this phenomenon on radiation doses increases with plan complexity and with range and period of target motion (Edvardsson et al. 2018). Consequently, the magnitude of the dose variation could change in each plan. In the treatment method applied in the present study, coldspots were not observed within ITV, in

contrast to hotspots. Hotspots (with doses $\geq 107\%$ of prescription dose) in ITV are allowed in SBRT applications and are preferred as compared to coldspots (with doses $\leq 95\%$ of the prescription dose). In addition, results of 3D in vivo EPID dosimetry measurements were in agreement with TPS doses, for static phantom irradiation. However, the pass rates for 3D measurements decreased dramatically for a moving phantom. This observation indicates that motion has a significant impact on dose distribution. Previously, Esposito and co-workers validated in vivo EPID dosimetry results for lung tumours using a static phantom (Esposito et al. 2021a, b). They reported good agreement between film and EPID doses. For moving targets, the results of in vivo transit dosimetry for SBRT treatments were reported in Esposito et al. 2021a, b. In this study, pre-treatment in-air irradiations showed overall good agreement between TPS and EPID dose distributions, using the 3%/3 mm criterion. However, in vivo results suggested systematically lower doses. This may be the reason why moving phantom passing rates were lower in gamma analysis (Esposito et al. 2021a, b). It is concluded that 3D dosimetry has advantages over point or 2D dosimetry.

Conclusion

The reconstructed density of the target depends on the method used for reconstruction. While any differences in density may cause a deviation in DVH parameters, they do not influence results of point measurements, 2D measurements, and 3D measurements for static phantom much. On the other hand, hotspots occurred and gamma analysis passing rates were significantly reduced when a mobile phantom was used. While 4DCT and 4D CBCT support a precise definition and visualization of the target, there are still dose uncertainties that are largely caused by target movement during irradiation. Experiments in this study suggest the use of MIP as a reconstruction method, 4D CBCT as setup imaging, and 3D dosimetry for dose verification in lung SBRT treatments.

Author contributions YY: performed the measurements; PH and GO: were involved in planning and supervised the work; YY and PH: processed the experimental data, performed the analysis, drafted the manuscript, and designed the figures. GO: aided in interpreting the results and worked on the manuscript. All authors discussed the results and commented on the manuscript.

Funding None.

Data availability The data that supports the findings of this study are available from the corresponding author upon reasonable request.

Declarations

Conflict of interest The authors have no conflicts of interest to disclose.

Ethical approval Not required.

References

- Admiraal MA, Schuring D, Hurkmans CW (2008) Dose calculations accounting for breathing motion in stereotactic lung radiotherapy based on 4D-CT and the internal target volume. *Radiother Oncol* 86(1):55–60
- Bradley JD, Nofal AN, El Naqa IM, Lu W, Liu J, Hubenschmidt J, Low DA, Drzymala RE, Khullar D (2006) Comparison of helical, maximum intensity projection (MIP), and averaged intensity (AI) 4D CT imaging for stereotactic body radiation therapy (SBRT) planning in lung cancer. *Radiother Oncol* 81(3):264–268
- Brandner ED, Chetty IJ, Giaddui TG, Xiao Y, Huq MS (2017) Motion management strategies and technical issues associated with stereotactic body radiotherapy of thoracic and upper abdominal tumors: A review from NRG oncology. *Med Phys* 44(6):2595–2612
- Chang JY, Senan S, Paul MA, Mehran RJ, Louie AV, Balter P, Groen HJM, McRae SE, Widder J, Feng L, van den Borne BEEM, Munsell MF, Hurkmans C, Berry DA, van Werkhoven E, Kresl JJ, Dingemans A-M, Dawood O, Haasbeek CJA, Carpenter LS, De Jaeger K, Komaki R, Slotman BJ, Smit EF, Roth JA (2015) Stereotactic ablative radiotherapy versus lobectomy for operable stage I non-small-cell lung cancer: a pooled analysis of two randomised trials. *Lancet Oncol* 16(6):630–637
- Childress NL, Rosen II (2003) The design and testing of novel clinical parameters for dose comparison. *Int J Radiat Oncol Biol Phys* 56(5):1464–1479
- Chopra KL, Harkenrider MM, Emami B, Melian E, Avadhani JS, Kehwar TS, Rai DV, Sethi A (2019) Impact of choice of dose calculation algorithm on PTV and OAR doses in lung SBRT. *J Radiat Oncol* 8(3):291–304
- Edvardsson A, Nordström F, Ceberg C, Ceberg S (2018) Motion induced interplay effects for VMAT radiotherapy. *Phys Med Biol* 63(8):085012
- Esposito M, Ghirelli A, Pini S, Alpi P, Barca R, Fondelli S, Grilli Leonulli B, Paoletti L, Rossi F, Bastiani P, Russo S (2021a) Clinical implementation of 3D in vivo dosimetry for abdominal and pelvic stereotactic treatments. *Radiother Oncol* 154:14–20
- Esposito M, Marrazzo L, Vanzi E, Russo S, Pallotta S, Talamonti C (2021b) A validation method for EPID in vivo dosimetry algorithms. *Appl Sci* 11(22):10715
- Giantsoudi D, De Man B, Verburg J, Trofimov A, Jin Y, Wang G, Gjestebj L, Paganetti H (2017) Metal artifacts in computed tomography for radiation therapy planning: dosimetric effects and impact of metal artifact reduction. *Phys Med Biol* 62(8):R49–R80
- Jiang B, Dai J, Zhang Y, Zhang K, Men K, Zhou Z, Liang J, Wang L (2012) Comparison of setup error using different reference images: a phantom and lung cancer patients study. *Med Dosim* 37(1):47–52
- Kubo K, Monzen H, Tamura M, Hirata M, Ishii K, Okada W, Nakahara R, Kishimoto S, Kawamorita R, Nishimura Y (2018) Minimizing dose variation from the interplay effect in stereotactic radiation therapy using volumetric modulated arc therapy for lung cancer. *J Appl Clin Med Phys* 19(2):121–127
- Liu Q, Liang J, Stanhope CW, Yan D (2016) The effect of density variation on photon dose calculation and its impact on intensity modulated radiotherapy and stereotactic body radiotherapy. *Med Phys* 43(10):5717–5729
- Low D (2015) The importance of 3D dosimetry. *J Phys Conf Ser*. <https://doi.org/10.1088/1742-6596/573/1/012009>
- Miften M, Olch A, Mihailidis D, Moran J, Pawlicki T, Molineu A, Li H, Wijesooriya K, Shi J, Xia P (2018) Tolerance limits and methodologies for IMRT measurement-based verification QA: recommendations of AAPM Task Group No. 218. *Med Phys* 45(4):e53–e83
- Mohatt DJ, Ma T, Wiant DB, Islam NM, Gomez J, Singh AK, Malhotra HK (2018) Technical and dosimetric implications of respiratory induced density variations in a heterogeneous lung phantom. *Radiat Oncol* 13(1):165
- Muirhead R, McNee SG, Featherstone C, Moore K, Muscat S (2008) Use of maximum intensity projections (MIPs) for target outlining in 4DCT radiotherapy planning. *J Thorac Oncol* 3(12):1433–1438
- Nakamura M, Narita Y, Matsuo Y, Narabayashi M, Nakata M, Yano S, Miyabe Y, Matsugi K, Sawada A, Norihisa Y, Mizowaki T, Nagata Y, Hiraoka M (2008) Geometrical differences in target volumes between slow CT and 4D CT imaging in stereotactic body radiotherapy for lung tumors in the upper and middle lobe. *Med Phys* 35(9):4142–4148
- Pan C-H, Shiau A-C, Li K-C, Hsu S-H, Liang J-A (2019) The irregular breathing effect on target volume and coverage for lung stereotactic body radiotherapy. *J Appl Clin Med Phys* 20(7):109–120
- Purdie TG, Bissonnette J-P, Franks K, Bezjak A, Payne D, Sie F, Sharpe MB, Jaffray DA (2007) Cone-beam computed tomography for on-line image guidance of lung stereotactic radiotherapy: localization, verification, and intrafraction tumor position. *Int J Radiat Oncol Biol Phys* 68(1):243–252
- Sarudis S, Karlsson A, Nyman J, Bäck A (2022) Dosimetric effects of respiratory motion during stereotactic body radiation therapy of lung tumors. *Acta Oncol* 61(8):1004–1011
- Schwarz M, Cattaneo GM, Marrazzo L (2017) Geometrical and dosimetric uncertainties in hypofractionated radiotherapy of the lung: a review. *Phys Med* 36:126–139
- Simone CB 2nd, Wildt B, Haas AR, Pope G, Rengan R, Hahn SM (2013) Stereotactic body radiation therapy for lung cancer. *Chest* 143(6):1784–1790
- Slotman BJ, Lagerwaard FJ, Senan S (2006) 4D imaging for target definition in stereotactic radiotherapy for lung cancer. *Acta Oncol* 45(7):966–972
- Sweeney RA, Seubert B, Stark S, Homann V, Müller G, Flentje M, Guckenberger M (2012) Accuracy and inter-observer variability of 3D versus 4D cone-beam CT based image-guidance in SBRT for lung tumors. *Radiat Oncol* 7:81
- Taremi M, Hope A, Dafele M, Pearson S, Fung S, Purdie T, Brade A, Cho J, Sun A, Bissonnette JP, Bezjak A (2012) Stereotactic body radiotherapy for medically inoperable lung cancer: prospective, single-center study of 108 consecutive patients. *Int J Radiat Oncol Biol Phys* 82(2):967–973
- Thengumpallil S, Smith K, Monnin P, Bourhis J, Bochud F, Moeckli R (2016) Difference in performance between 3D and 4D CBCT for lung imaging: a dose and image quality analysis. *J Appl Clin Med Phys* 17(6):97–106
- Tian Y, Wang Z, Ge H, Zhang T, Cai J, Kelsey C, Yoo D, Yin FF (2012) Dosimetric comparison of treatment plans based on free breathing, maximum, and average intensity projection CTs for lung cancer SBRT. *Med Phys* 39(5):2754–2760
- Timmerman RD, Paulus R, Pass HI, Gore E, Edelman MJ, Galvin JM, Choy H, Straube W, Nedzi LA, McGarry R (2013) RTOG 0618: stereotactic body radiation therapy (SBRT) to treat operable early-stage lung cancer patients. *J Clin Oncol*. https://doi.org/10.1200/jco.2013.31.15_suppl.7523
- Underberg RW, Lagerwaard FJ, Cuijpers JP, Slotman BJ, van Sörnsen JR, de Koste and S. Senan, (2004) Four-dimensional CT scans for

- treatment planning in stereotactic radiotherapy for stage I lung cancer. *Int J Radiat Oncol Biol Phys* 60(4):1283–1290
- Underberg RW, Lagerwaard FJ, Slotman BJ, Cuijpers JP, Senan S (2005) Use of maximum intensity projections (MIP) for target volume generation in 4DCT scans for lung cancer. *Int J Radiat Oncol Biol Phys* 63(1):253–260
- Underberg RW, Lagerwaard FJ, Van Tinteren H, Cuijpers JP, Slotman BJ, Senan S (2006) Time trends in target volumes for stage I non-small-cell lung cancer after stereotactic radiotherapy. *Int J Radiat Oncol Biol Phys* 64(4):1221–1228
- Vedam SS, Keall PJ, Kini VR, Mostafavi H, Shukla HP, Mohan R (2002) Acquiring a four-dimensional computed tomography dataset using an external respiratory signal. *Phys Med Biol* 48(1):45–62
- Wang W, Chen D, Han C, Zheng X, Zhou Y, Gong C, Xie C, Jin X (2018) Partial and full arc volumetric modulated arc therapy in lung cancer stereotactic body radiotherapy with different definitions of internal target volume based on 4D CT. *Intern J Med Phys Clin Eng Radiation Oncol* 7(04):491
- Yedekci Y, Biltekin F, Ozyigit G (2019) Feasibility study of an electronic portal imaging based in vivo dose verification system for prostate stereotactic body radiotherapy. *Physica Med* 64:204–209
- Zamora DA, Riegel AC, Sun X, Balter P, Starkschall G, Mawlawi O, Pan T (2010) Thoracic target volume delineation using various maximum-intensity projection computed tomography image sets for radiotherapy treatment planning. *Med Phys* 37(11):5811–5820
- Zhi S, Kachelrieß M, Mou X (2020) High-quality initial image-guided 4D CBCT reconstruction. *Med Phys* 47(5):2099–2115

Publisher's Note Springer Nature remains neutral with regard to jurisdictional claims in published maps and institutional affiliations.

Springer Nature or its licensor (e.g. a society or other partner) holds exclusive rights to this article under a publishing agreement with the author(s) or other rightsholder(s); author self-archiving of the accepted manuscript version of this article is solely governed by the terms of such publishing agreement and applicable law.